Int. J. Electrochem. Sci., 16 **(2021)** Article ID: 210820, doi: 10.20964/2021.08.25

International Journal of
ELECTROCHEMICAL
SCIENCE
www.electrochemsci.org

Synthesis and Study of Magnesium Ferrite/Reduced Graphene Oxide ($MgFe_2O_4$/rGO) Nanocomposite Electrodes to Electrochemical Removal of Hexavalent Chromium Ion from Wastewater

Bangjun Han[1], *Renzheng Gu*[1], *Xingya Wei*[1], *Xueyan Li*[2,*]

[1]School of Civil and Transportation Engineering, Shanghai Urban Construction Vocational College, 200438 Shanghai, P. R. China.
[2]School of Environmental Science and Engineering, Suzhou University of Science and Technology, 215009 Suzhou, P. R. China
[*]E-mail: lixueyan@usts.edu.cn

Received: 8 April 2021/ *Accepted:* 28 May 2021 / *Published:* 30 June 2021

This study was conducted on the synthesis of magnesium ferrite/reduced graphene oxide ($MgFe_2O_4$/rGO) nanocomposite as anodes for removal of hexavalent chromium (Cr(VI)) ions from industrial wastewater through the electrocoagulation (EC) technique. $MgFe_2O_4$/rGO was synthesized using a hydrothermal method. Study of the morphology surface $MgFe_2O_4$/rGO using SEM showed that the $MgFe_2O_4$ particles were strongly attached on 3D crumpled and rippled rGO nanosheets which illustrated the higher porosity of the $MgFe_2O_4$/rGO structure. XRD analysis also indicated good anchoring of $MgFe_2O_4$ particles on rGO nanosheets. Results of EIS studies prove the interfacial processes and lower charge transfer resistance of $MgFe_2O_4$/rGO than that of $MgFe_2O_4$. The effect of pH value, Cr (VI) concentration and current density was studied for removal of Cr (VI) from industrial wastewater using the $MgFe_2O_4$/rGO as anode via EC technique. Results showed that complete treatment was obtained for treatment of 60 mg/L of Cr (VI) in NaCl concentration of 0.4 g/L and pH 2 under 25 minutes EC for 5mA/cm^2 current density and energy consumption of 0.0072 kWh/m^3. Comparison between obtained results for Cr(VI) treatment using $MgFe_2O_4$/rGO nanocomposite and other reported works indicated to lower energy consumption in this study due lower charge transfer resistance in $MgFe_2O_4$/rGO.

Keywords: Ferrite; Reduced Graphene; Nanocomposite; Hexavalent Chromium; EC

1. INTRODUCTION

Hexavalent chromium (Cr(VI)), the most toxic form of chromium, exhibits unique physical and chemical properties such as high corrosion resistance, color, durability, and hardness, making Cr(VI) based compounds the most in demand in a wide range of industrial applications such as chrome plating, plastics, photo engraving, automobiles, stainless steel and super alloys, leather tanning, and ink printing [1, 2]. Therefore, a large amount of chromium compounds have been entering into the sewage system and industrial waste every year.

Studies show the long-term inhalation of Cr(VI) can cause liver damage, lung cancer, asthma, dermatitis, eczema, birth defects and many reproductive harms [3, 4]. Therefore, the treatment of Cr(VI) compounds from industrial waste is indispensable due to its mutagenicity and carcinogenicity based on prevention and control of environmental pollution laws in most countries [5, 6].

Accordingly, many studies have been performed based on membrane filtration, neutralization, ion exchange, chemical precipitation, flotation, adsorption, electrocoagulation (EC), photocatalytic and electrochemical reduction techniques for removing Cr(VI) compounds from industrial wastewaters [7-13]. However, many of these techniques are expensive, complicated and consume large amounts of chemicals, energy and time. EC as an electrochemical technique has been shown in studies to be a new practical, low-cost, and efficient method for treating water and industrial effluents.

Therefore, these studies were carried out for synthesis and study the magnesium ferrite/ reduced graphene oxide ($MgFe_2O_4$/rGO) nanocomposite electrodes for electrochemical removal of Cr(VI) ion from industrial wastewater.

2. MATERIALS and METHOD

For synthesis the $MgFe_2O_4$/rGO using hydrothermal method [14], 7mM iron nitrate (99%, XiaxianYunli Chemicals Co., Ltd., China), 3mM magnesium nitrate (99%, Xilong Scientific Co., Ltd., China), and 6mM citric acid (99%, Hebei Qige Biotechnology Co., Ltd., China) were mixed in 25 ml of deionized (DI) water under magnetic stirring at 50°C for 15 minutes. Then, rGO (≥75 wt.% Carbon, Sigma-Aldrich) was ultrasonically dispersed in solution at a mass ratio of 20% wt. After that, the resulting suspension was transferred to a 50ml Teflon-lined stainless-steel autoclave and dried at 100°C for 5 hours. After cooling, the products were collected by vacuum filtration and ultrasonically rinsed with DI water and ethanol, respectively, and then dried in an oven at 70°C for 30 minutes.

The surface morphology of $MgFe_2O_4$ and $MgFe_2O_4$/rGO was studied by scanning electron microscopy (SEM, JEOL-JSM-6010LA, Tokyo, Japan). The crystalline structures of prepared anodes were analyzed by X-ray diffraction (XRD, CuKα radiation ($\lambda = 1.5418$ Å), Ultima-IV; Rigaku, Japan). Electrochemical impedance spectroscopy (EIS) measurements were conducted on potentiostat/galvanostat (3000 ZRA, Gamry, Warminster, PA, USA) in a conventional three-electrode electrochemical cell consisting of the prepared samples as working electrode, Ag/AgCl electrode as the reference electrode and Pt plate as counter electrode. electrochemical measurements were recorded in 0.5 M sodium nitrate ($NaNO_3$, ≥99.0%, Sigma-Aldrich) electrolyte in an ac frequency range of 0.1 Hz to 100 KHz at open circuit potential with an amplitude of 5 mV.

The wastewater sample was collected from Beijing's Industrial Wastewater. The wastewater was filtered and centrifuged at 1500 rpm for 15 minutes. The resulted supernatant was characterized using the standard procedure prescribed by the American Public Health Association (APHA) [15]. The results of wastewater sample characterization are given in Table 1.

The EC treatment was performed in the reactor which contained a 100 ml beaker and stainless steel sheet as cathode and $MgFe_2O_4$ or $MgFe_2O_4$/rGO as anode with dimensions of 1.5 cm × 5 cm × 2 mm. The inter-electrode distance was adjusted at 1.5cm. For 30 minutes, the electrode was connected to a DC power supply with a current density of 2-12mA/cm^2 via a DC power supply (TEK-8051, 30 V and 5 A) and an applied voltage of 2.8 V. 0.4 g/L NaCl (99%, Shanghai Sky Chem Industrial Co., Ltd, China) solution was used as the supporting electrolyte. The adjustment of pH of the electrolyte was performed with HCl and NaOH solutions using a pH meter (HANNA Instruments, China). At interval times, the concentration of Cr (VI) of electrocoagulated samples were analyzed according to the standard methods using UV-visible spectrophotometer (Shimadzu UV-2550 double beam, $\lambda = 540$ nm, Japan). The removal efficiency and energy consumption were obtained using the following equations (1) and (2), respectively [16]:

$$\text{Removal efficiency} = \frac{C_0 - C_t}{C_0} \times 100 \qquad (1)$$

$$\text{Energy consumption} = \frac{UIt}{60\,V} \qquad (2)$$

Where C_0 (g/l) and C_t (g/l) are the initial concentration of Cr(VI) in the initial solution and electrocoagulated sample, respectively. U (V), I (A),t (minute) and V (m^3) are the mean applied voltage, current, the treatment time and the sample volume, respectively.

Table 1. Detail of Initial characteristics of the wastewater sample.

Property	Value
TOC	28.2 mg/l
COD	33.3 mg/l
Cr (VI)	60 mg/l
Ni	4.7 mg/l
Lead	6.9 mg/l
pH	4.9
conductivity	7.1 mS/cm

3. RESULTS AND DISCUSSION

3.1. Structural and electrochemical characterization of $MgFe_2O_4$ and $MgFe_2O_4$/rGO

SEM images in Figure 1 show the morphology of $MgFe_2O_4$ and $MgFe_2O_4$/rGO which indicates heterogeneously aggregation of particles in the photocatalyst matrix. The $MgFe_2O_4$ (Figure 1a) contains a large number of hexahedron shaped particles with an average size of 75 nm. $MgFe_2O_4$/rGO

(Figure 1b) shows that the $MgFe_2O_4$ particles are strongly attached to the 3D crumpled and rippled rGO nanosheets, which illustrated the higher porosity of the $MgFe_2O_4$/rGO structure. The high porous network increases the specific surface area that it can provide to the higher charge storage capability while also making the electrode surface easily accessible to the electrolyte ions [17-20].

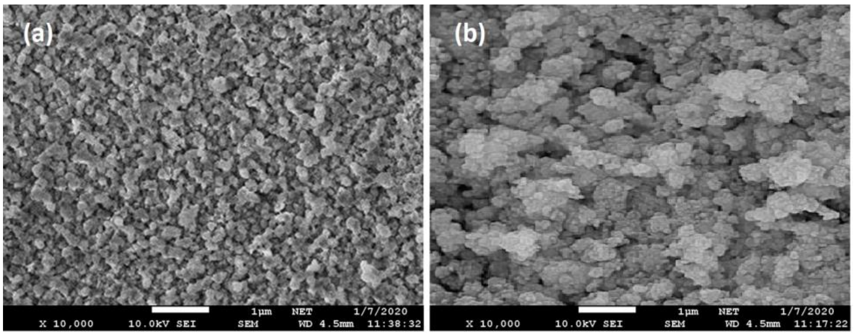

Figure 1. SEM images of (a) $MgFe_2O_4$ and (b) $MgFe_2O_4$/rGO.

XRD patterns in Figure 2 show the crystalline structure of $MgFe_2O_4$ and $MgFe_2O_4$/rGO. XRD pattern of rGO shows two diffraction peaks at 26.39° and 42.59° which indicated to (002) and (004) planes of graphite, respectively (JCPDS card No. 75-1621). XRD pattern of $MgFe_2O_4$ shows the diffraction peaks at 29.33°, 35.41°, 40.51°, 49.04°, 53.11°, 57.21°, 62.20°, 63.66°, and 71.54° which indicated to face centered cubic of $MgFe_2O_4$ with (220), (400), (422), (201), (422), (511), (444), (440), and (533) planes (JCPDS card No. 89-4924), respectively. The XRD pattern of $MgFe_2O_4$/rGO displays not only the diffraction peak of (002) plane of rGO but also shows the diffraction peaks of $MgFe_2O_4$, implying the good anchoring of $MgFe_2O_4$ particles on rGO nanosheets.

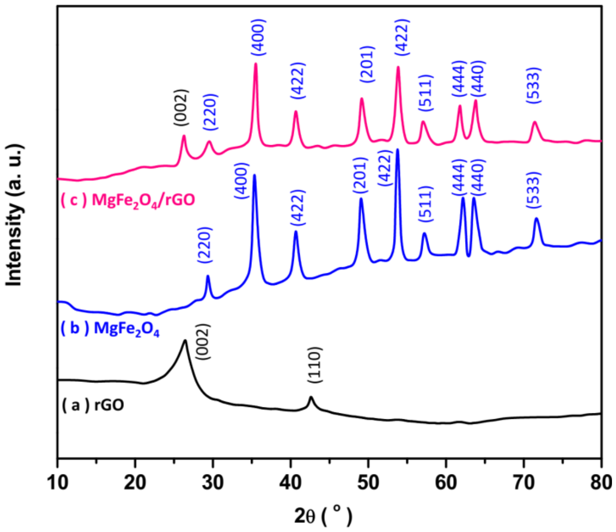

Figure 2. XRD patterns of (a) rGO, (b) $MgFe_2O_4$ and (c) $MgFe_2O_4$/rGO.

EIS measurements were performed on 0.5 M $NaNO_3$ electrolyte in the ac frequency range of 0.1 Hz to 100 KHz at open circuit potential with an amplitude of 5 mV to investigate the electrical conductivity of the prepared photocatalyst. Figure 3 shows the lower diameter of the semicircle of $MgFe_2O_4$/rGO nanocomposite than $MgFe_2O_4$ electrode which is attributed to the interfacial processes and lower charge transfer resistance (R_{ct}) of nanocomposite in high frequency [21, 22]. Therefore, incorporation of rGO in nanocomposite acts as a conductive support for $MgFe_2O_4$ nanoparticles and decreases the R_{ct} value from 30.2 to 10.5 Ω, which can be assigned to facile transition of electrons [23]. Thus, the $MgFe_2O_4$/rGO nanocomposite represented the fast electron transport in electrochemical reaction, and thereby higher treatment rate of Cr(VI) because of the synergistic effect between $MgFe_2O_4$ nanoparticles and rGO nanosheets [21, 23].

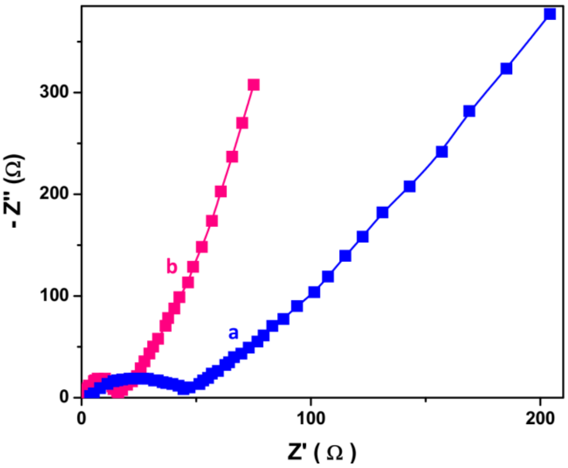

Figure 3. EIS measurements of of (a) $MgFe_2O_4$ and (b) $MgFe_2O_4$/rGO in 0.5 M $NaNO_3$ electrolyte in ac frequency range of 0.1 Hz to 100 KHz at open circuit potential with amplitude of 5 mV.

3.2. Treatment of wastewater by EC

pH is the most important factor that influences the performance of the electrochemical removal process of chromium [23]. The effect of initial pH on the Cr(VI) treatment by electrochemical process with $MgFe_2O_4$ and $MgFe_2O_4$/rGO electrodes are shown in Figures 4a and 4b, respectively. As seen during 30 minutes of electrochemical treatment, the Cr (VI) removal efficiency of $MgFe_2O_4$ and $MgFe_2O_4$/rGO electrodes increased from 88.66% to 97.98% and from 92.41% to 100.00%, respectively with decreasing the initial pH value from 10 to 2. Therefore, the results indicate better removal of Cr(VI) in the acidic media because of the contribution of more hydrogen ion in the acidic electrolyte to formation of additional possible reaction pathways for treatment of Cr(VI) [24]. Hydrogen ion leads to remarkably strong electrostatic attraction between Cr(VI) ions and the positively charged particle surface that can also facilitate the reduction of Cr(VI) ions to Cr(III) [25]. Moreover, it can be found from Figure 4a and 4b that the removal efficiency of $MgFe_2O_4$/rGO electrode is higher than $MgFe_2O_4$ in all pH values, which is in agreement with the SEM and EIS results. Therefore, the following studies were conducted on $MgFe_2O_4$/rGO electrode.

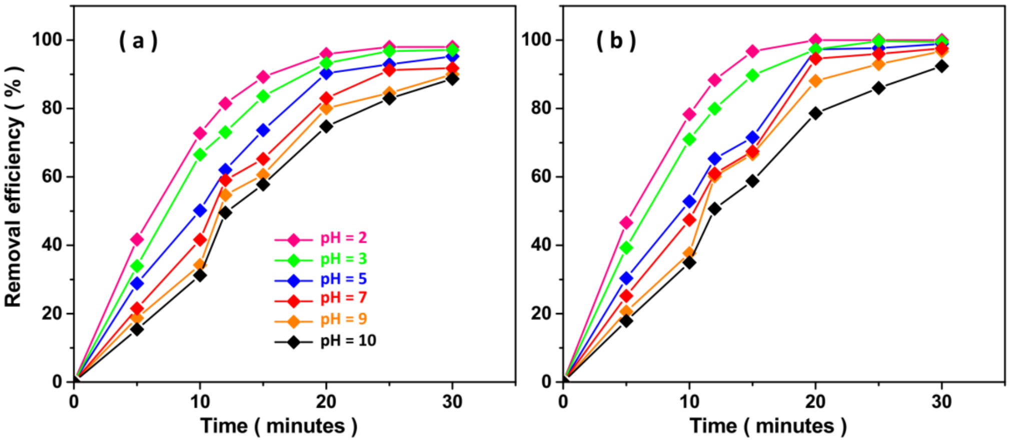

Figure 4. Initial pH Effects on removal of Cr(VI) in 5mA/cm^2 current density, and 0.4g/L NaCl concentration and initial Cr(VI) concentration of 60mg/L using stainless steel sheet as cathode and (a) $MgFe_2O_4$ and (b) $MgFe_2O_4$/rGO as anodes.

The initial concentration of Cr(VI) on the removal efficiency of $MgFe_2O_4$/rGO anode was also investigated. Figure 5 shows the removal efficiency of different initial concentrations of Cr (VI) solutions from 30 to 250 mg/L at a current density of 5mA/cm^2, and 0.4g/L NaCl concentration and pH 2. After 30 minutes of electrochemical treatment, the removal efficiencies of initial concentrations of 30, 60, 100, 150, 200, and 250 mg/L of Cr(VI) solutions are 100.0%, 100.0%, 93.40%, 64.64%, 55.93%, and 45.91%, respectively. It indicates the removal efficiency is decreased with increasing the initial concentration of Cr(VI) which is attributed to Faraday's law [26, 27]. This law exhibits that when current density is constant, a constant number of Fe^{2+} is released to the solution, and consequently Fe^{2+} is not sufficient for the reduction reaction for high concentration of Cr(VI) [26, 27]. Furthermore, it can be related to saturation of higher energy sites of anode in high concentration of Cr(VI) [28].

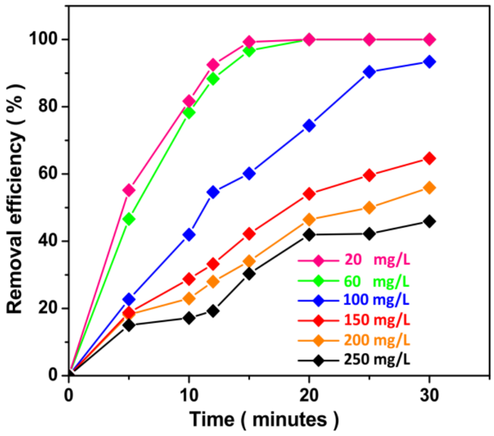

Figure 5. Effect of initial concentration of Cr(VI) on the removal efficiency of $MgFe_2O_4$/rGO as anodes and stainless steel sheet as cathodes in 5mA/cm^2 current density, and 0.4 g/L NaCl concentration and pH 2

Current density has a main role in electrochemical treatment processes and energy consumption that could determine the removal performance and operational costs. Current density shows the strong effect on the flock's formation rate and on the amount and size of the produced bubbles [29, 30]. Figure 6 shows the changes in the Cr (VI) removal efficiency on $MgFe_2O_4$/rGO in terms of current density for initial Cr (VI) concentration of 60 mg/L in NaCl concentration of 0.4 g/L and pH 3. As seen, Cr(VI) removal efficiency of Cr(VI) reaches 96.48% at current density of 2mA/cm^2 after 30 minutes. In addition, the complete removal is obtained after 25, 20, 15 and 12 minutes of electrochemical treatment for current densities of 5, 8, 10 and 12mA/cm^2, respectively. It is proposed that increasing the current density increases the removal rate, which is related by a direct proportional relationship between the potential of electrolysis and current density [29], indicating it may associated with enhance the creation and reaction with hydroxyl radicals and increase the release of Fe^{2+} from anode which implied to generation of more ferrous hydroxides [30].

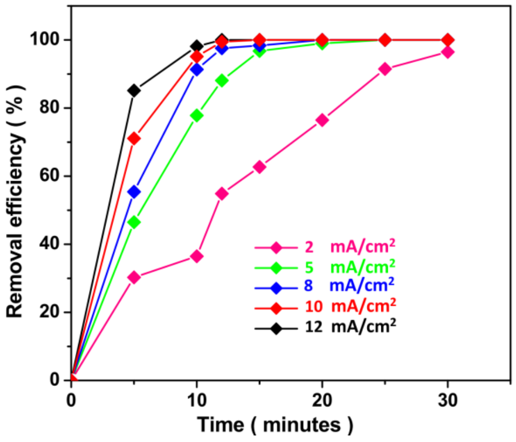

Figure 6. Changes in the Cr (VI) removal efficiency on $MgFe_2O_4$/rGO as anodes and stainless steel sheet as cathodes in terms of current density for initial Cr(VI) concentration of 60mg/L in NaCl concentration of 0.4 g/L and pH 2

Figure 7 displays the variation of energy consumption toward various current densities ranging from 2 to 12mA/cm^2 for an initial Cr(VI) concentration of 60 mg/L in NaCl concentration of 0.4 g/L and pH 2, demonstrating that increasing the energy consumption with increasing the current density. As seen after 30 minutes treatment, the energy consumption values are obtained from 0.0035 to 0.0200kWh/m^3 as current densities increased from 2 to 12mA/cm^2.

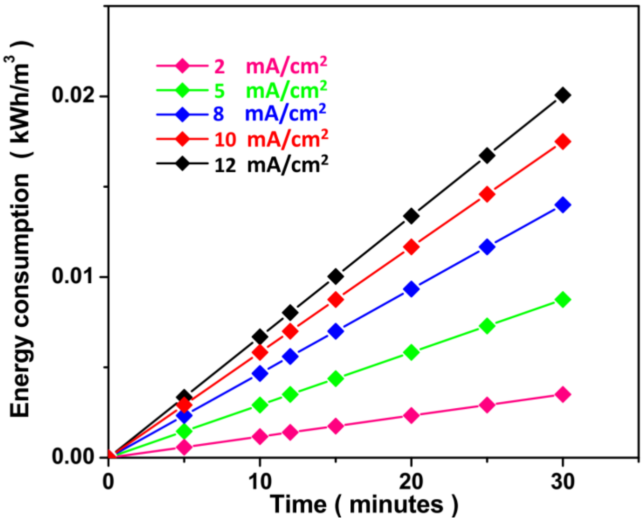

Figure 7. Variation of the energy consumption on $MgFe_2O_4$/rGO as anodes and stainless steel sheet as cathodes toward various current density for initial Cr(VI) concentration of 60mg/L in NaCl concentration of 0.4 g/L and pH 2.

Table 1. Comparison between obtained results for electrochemical removal Cr (VI) using $MgFe_2O_4$/rGO as anode and other studies

Electrode material	pH	Initial Cr (VI) concentration (mg/L)	Current density (mA/cm^2)	Removal efficiency (%)	Time (minute)	Energy consumption (kWh/m^3)	Ref.
Fe	3	75	200	100	5	22.07	[31]
Fe	4.66	40	2.03	56.3	14	0.0450	[27]
Fe	8	100	1.002	94.97	40	1.5328	[32]
Al	3	75	200	100	10	59.34	[31]
Fe-Fe	8	39	-	96.2	30	51.40	[33]
Fe-Fe	6	106	0.73	95.76	50	0.63	[34]
Fe-Al	3	44.5	10	100	20	10.07	[35]
Al-Fe	5	100	150	98	25	16.30	[36]
MC/Fe_3O_4@PPy*	3	50	5.66	99.87	20	0.6274	[37]
Cu	5.66	100	4.132	95.21	40	1.228	[38]
$MgFe_2O_4$/rGO	2	60	2 5	100 100	30 25	0.0035 0.0072	This work

* Microbial cellulose /Fe_3O_4@ polypyrrole

Table 1 exhibits a comparison between obtained results for electrochemical removal Cr(VI) using $MgFe_2O_4$/rGO as anode and other studies. As seen, the obtained energy consumption in this study is lower than other electrochemical treatment studies based on Cu, Fe, Al and Fe-Al anodes. Moreover, the removal efficiency values are also higher than in other studies. This can be due to lower charge transfer resistance in $MgFe_2O_4$/rGO, which decreases the voltage drop at constant current density.

In order to study the stability and durability of proposed anode, the removal efficiency of the $MgFe_2O_4$/rGO was evaluated at 5 mA/cm^2 for an initial Cr(VI) concentration of 60 mg/L in NaCl concentration of 0.4 g/L and pH 2. Figure 8 shows that after five reuses, removal efficiency decreases by 8%, 4.8%, 4.5%, 5%, 3.5%, and 2.1% after 5, 10, 15, 20, 25, and 30 minutes of treatment, respectively. It can be related to a decrease of Cr(VI) adsorption and decline of ferrous hydroxide formation [39]. Studies have been shown that use of high-concentration NaOH solutions can increase the hydroxide ion concentration and improve the reaction backwards [40].

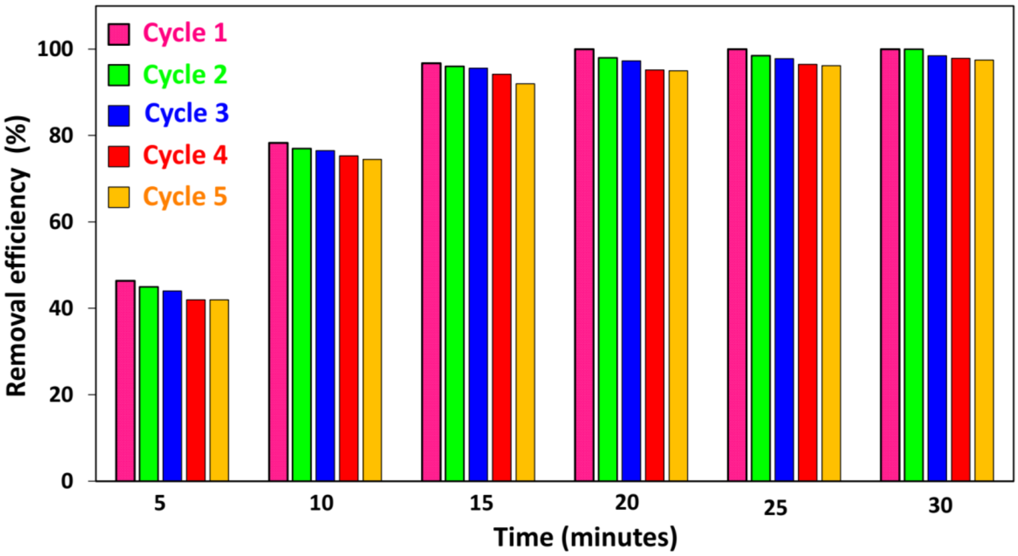

Figure 8. Removal efficiency of reused $MgFe_2O_4$/rGO at 5 mA/cm^2 for initial Cr(VI) concentration of 60 mg/L in NaCl concentration of 0. 4 g/L and pH 2.

4. CONCLUSION

This study presented synthesis of$MgFe_2O_4$/rGO nanocomposite and application as anodes for removal of Cr(VI) from industrial wastewater through the EC technique. The hydrothermal method was applied to the synthesis of $MgFe_2O_4$/rGO. Results of studies of morphology and structure of nanocomposite indicated good anchoring of $MgFe_2O_4$ particles on rGO nanosheets. Results of EIS studies prove the interfacial processes and lower charge transfer resistance of $MgFe_2O_4$/rGO than that of $MgFe_2O_4$. EC treatment of Cr(VI) from industrial wastewater using the $MgFe_2O_4$/rGO was performed to investigation of the effect of pH value, Cr(VI) concentration and current density. Results showed that 100.0% removal efficiency was obtained for treatment of 60 mg/L of Cr(VI) in NaCl concentration of 0.4 g/L and pH 2 under 25 minutes EC for current densities of 5 and energy consumption of 0.0072 kWh/m^3. Comparison between obtained results for electrochemical removal Cr(VI) using $MgFe_2O_4$/rGO nanocomposite and other studies indicated lower energy consumption in this study due to fast electron transport of nanocomposite and synergistic effect between $MgFe_2O_4$ nanoparticles and rGO nanosheets

References

1. M. Kendig, S. Jeanjaquet, R. Addison and J. Waldrop, *Surface and Coatings Technology*, 140 (2001) 58.
2. H. Karimi-Maleh, Y. Orooji, A. Ayati, S. Qanbari, B. Tanhaei, F. Karimi, M. Alizadeh, J. Rouhi, L. Fu and M. Sillanpää, *Journal of Molecular Liquids*, 329 (2021) 115062.
3. M. Cieślak-Golonka, *Polyhedron*, 15 (1996) 3667.
4. C. Liu and J. Rouhi, *RSC Advances*, 11 (2021) 9933.
5. H. Karimi-Maleh, M. Alizadeh, Y. Orooji, F. Karimi, M. Baghayeri, J. Rouhi, S. Tajik, H. Beitollahi, S. Agarwal and V.K. Gupta, *Industrial & Engineering Chemistry Research*, 60 (2021) 816.
6. J. Rouhi, H.K. Malayeri, S. Kakooei, R. Karimzadeh, S. Alrokayan, H. Khan and M.R. Mahmood, *International Journal of Electrochemical Science*, 13 (2018) 9742.
7. H. Peng and J. Guo, *Environmental Chemistry Letters*, 18 (2020) 2055.
8. Y. Zhao, D. Kang, Z. Chen, J. Zhan and X. Wu, *International Journal of Electrochemical Science*, 13 (2018) 1250.
9. S. Li, Z. Hu, S. Xie, H. Liu and J. Liu, *International Journal of Electrochemical Science*, 13 (2018) 655.
10. H. Karimi-Maleh, Y. Orooji, F. Karimi, M. Alizadeh, M. Baghayeri, J. Rouhi, S. Tajik, H. Beitollahi, S. Agarwal and V.K. Gupta, *Biosensors and Bioelectronics*, 184 (2021) 113252.
11. G.-X. Li, H.-C. Yang, S. Guo, C.-F. Qi, K.-J. Wu and F.-F. Guo, *International Journal of Electrochemical Science*, 15 (2020) 6143.
12. S. Zhang, X. Yang, X. Cheng, C. Hu, B. Chai, J. Li and Y. Mei, *International Journal of Electrochemical Science*, 11 (2016) 5753.
13. H. Karimi-Maleh, M.L. Yola, N. Atar, Y. Orooji, F. Karimi, P.S. Kumar, J. Rouhi and M. Baghayeri, *Journal of colloid and interface science*, 592 (2021) 174.
14. M.L. Baynosa, A.H. Mady, D.R. Kumar, M.S. Sayed, D. Tuma and J.-J. Shim, *Journal of colloid and interface science*, 561 (2020) 459.
15. A.P.H. Association, A.W.W. Association, W.P.C. Federation and W.E. Federation, *Standard methods for the examination of water and wastewater*. Vol. 2. 1912: American Public Health Association.
16. R. Niazmand, M. Jahani, F. Sabbagh and S. Rezania, *Water*, 12 (2020) 1687.
17. N.F. Sylla, N.M. Ndiaye, B.D. Ngom, D. Momodu, M.J. Madito, B.K. Mutuma and N. Manyala, *Scientific Reports*, 9 (2019) 13673.
18. K. Kierzek and G. Gryglewicz, *Molecules*, 25 (2020) 4255.
19. H. Savaloni, E. Khani, R. Savari, F. Chahshouri and F. Placido, *Applied Physics A*, 127 (2021) 1.
20. F. Chahshouri, H. Savaloni, M. Khoramshahi and R. Savari, *3rd International Biennial Oil, Gas and Petrochemical Conference*, 1 (2020) 12.
21. S. Aralekallu, M. Palanna, S. Hadimani, K. Prabhu C. P, V.A. Sajjan, M.O. Thotiyl and L.K. Sannegowda, *Dalton Transactions*, 49 (2020) 15061.
22. H. Gul, A.-u.-H.A. Shah and S. Bilal, *Polymers*, 11 (2019) 1678.
23. P. Cao, J. Peng, S. Liu, Y. Cui, Y. Hu, B. Chen, J. Li and M. Zhai, *Scientific reports*, 7 (2017) 1.
24. Ihsanullah, F.A. Al-Khaldi, B. Abu-Sharkh, A.M. Abulkibash, M.I. Qureshi, T. Laoui and M.A. Atieh, *Desalination and Water Treatment*, 57 (2016) 7232.
25. A.A. Attia, S.A. Khedr and S.A. Elkholy, *Brazilian Journal of Chemical Engineering*, 27 (2010) 183.
26. G. Selvabharathia, S. Adishkumarb and J.R. Banuc, *Desalination and Water Treatment*, 156 (2019) 340.

27. Y.A. El-Taweel, E.M. Nassef, I. Elkheriany and D. Sayed, *Egyptian journal of petroleum*, 24 (2015) 183.
28. S. Hussain, S. Gul, S. Khan and H. ur Rehman, *Arabian Journal of Geosciences*, 6 (2013) 4547.
29. S.T. McBeath, D.P. Wilkinson and N.J. Graham, *Environmental Science: Water Research & Technology*, 6 (2020) 2405.
30. R. Jobby, P. Jha, A.K. Yadav and N. Desai, *Chemosphere*, 207 (2018) 255.
31. K. Cheballah, A. Sahmoune, K. Messaoudi, N. Drouiche and H. Lounici, *Chemical Engineering and Processing: Process Intensification*, 96 (2015) 94.
32. T. Zewail and N. Yousef, *Journal of Electroanalytical Chemistry*, 735 (2014) 123.
33. D. Bhagawan, S. Poodari, T. Pothuraju, D. Srinivasulu, G. Shankaraiah, M. Yamuna Rani, V. Himabindu and S. Vidyavathi, *Environmental Science and Pollution Research*, 21 (2014) 14166.
34. J. Lu, Z.-R. Wang, Y.-L. Liu and Q. Tang, *Process Safety and Environmental Protection*, 104 (2016) 436.
35. F. Akbal and S. Camcı, *Desalination*, 269 (2011) 214.
36. E. Keshmirizadeh, S. Yousefi and M.K. Rofouei, *Journal of hazardous materials*, 190 (2011) 119.
37. N.S. Marghaki, Z.A. Jonoush and A. Rezaee, *Journal of Cleaner Production*, 277 (2020) 123195.
38. S.R. Patel and S.P. Parikh, *Arabian Journal of Chemistry*, 13 (2020) 7032.
39. K.Z. Elwakeel, A.M. Elgarahy, Z.A. Khan, M.S. Almughamisi and A.S. Al-Bogami, *Materials Advances*, 1 (2020) 1546.
40. M. Liang, Y. Ding, Q. Zhang, D. Wang, H. Li and L. Lu, *Scientific Reports*, 10 (2020) 21473.